Inorganic Chemistry

Article

pubs.acs.org/IC

The Modulated Structure of $Co_3Al_4Si_2$: Incommensurability and Co−Co Interactions in Search of Filled Octadecets

Rie T. Fredrickson and Daniel C. Fredrickson*

Department of Chemistry, University of Wisconsin−Madison, 1101 University Avenue, Madison, Wisconsin 53706, United States

Supporting Information

ABSTRACT: Incommensurate modulations are increasingly being recognized as a common phenomenon in solid-state compounds ranging from inorganic materials to molecular crystals. The origins of such modulations are often mysterious, but appear to be as diverse as the compounds in which they arise. In this Article, we describe the crystal structure and bonding of $Co_3Al_4Si_2$, the δ phase of the Co−Si−Al system, whose modulated structure can be traced to a central concept of inorganic chemistry: the 18 electron rule. The structure is monoclinic, conforming to the 3 + 1D superspace group $C/2m(0\beta0)s0$. The basis of the crystal structure is a rod packing of columns of the fluorite (CaF_2) type, a theme that is shared by the recently determined structure of $Fe_8Al_{17.4}Si_{7.6}$. The columns are arranged into sheets, within which the fluorite structure's primitive cubic network of Si/Al atoms continues uninterrupted from column to column. Between the sheets, layers of interstitial Si/Al atoms occur, some of which are arranged with a periodicity incommensurate with that of the fluorite-type columns. Strong modulations in the interstitial layers result. Electronic structure calculations, using a DFT-calibrated Hückel model on a commensurate approximate structure, reveal that the complex pattern of atoms within these interstitial layers serves to distribute Si/Al atoms around the Co atoms in order to reach 18 electron counts (filled octadecets). Central to this bonding scheme is the covalent sharing of electron pairs between Co atoms. The shared electron pairs occupy orbitals that are isolobal to classical Co−Co σ and π bonds, but whose stability is tied to multicenter character involving bridging Si/Al atoms. Through these features, $Co_3Al_4Si_2$ expands the structural and electronic manifestations of the 18 electron rule in solid-state inorganic compounds.

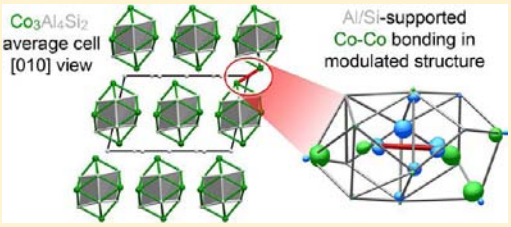

1. INTRODUCTION

The electronic properties of transition metal (TM) silicides have led to widespread applications as semiconductor materials.[1] Narrow band gaps or deep pseudogaps in the electronic density of states (DOS) curve at the Fermi energy (E_F) underlie the semiconducting (or poorly metallic) nature of these compounds.[2] Such indications of electronic stability are often accompanied by complex structures, such as helical motifs, as in the Nowotny Chimney Ladder phases,[3] or superstructures arising from vacancies, as in Re_4Si_7.[4] The coincidence of these complicated crystal structures with moderate conductivities provides one rationale for the promising thermoelectric properties of many silicide phases,[5] in the framework of the phonon-glass, electron-crystal model.[6] The relationship between the structural chemistry and electronic properties of silicides is thus of central importance, but a general bonding scheme that connects these intriguing structural features to DOS minima at prescribed electron counts remain elusive. The determination of such a universal bonding scheme for these compounds could be transformative in the design of new silicon-based materials.

Clues to the structure−electronics connection in these materials were recently found in the crystal structure and bonding analysis of $Fe_8Al_{17.4}Si_{7.6}$.[7] In this phase, columns of the simple fluorite-type structure (as adopted by the silicides $CoSi_2$[8] and $NiSi_2$[9]) occur in a rod packing, separated by single-atom-thick interface layers (Figure 1). As in many silicides, the DOS curve for this phase exhibits a pseudogap at the E_F, but in this case, a simple explanation was possible. In the fluorite-type phases $CoSi_2$ and $NiSi_2$, the TM atoms interact with their surrounding Si atoms in a fashion that is nearly isolobal with a TM coordination complex; the DOS pseudogap coincides with an 18 electron configuration on the TM sites (or filled octadecet by analogy with the octet rule). In moving to the Fe−Si−Al system, the incorporation of Fe on the TM sites and Al on some of the Si sites would deplete electrons from this filled octadecet, destabilizing the fluorite type. The fragmentation of the fluorite structure in $Fe_8Al_{17.4}Si_{7.6}$ allows additional Al atoms into the TM coordination environments to restore their 18 electron counts.

The evocation of the 18 electron rule in $Fe_8Al_{17.4}Si_{7.6}$ hints that this classic principle of TM chemistry may provide a more general explanation of the band gaps and DOS pseudogaps in TM−silicon-based materials. Indeed, a similar scheme was earlier proposed for half-Heusler phases.[10] A challenge to extending this picture, however, is the frequent occurrence of TM−TM contacts in many compounds that cannot simply be neglected in the bonding analysis. In this Article, we present the crystal structure and theoretical analysis of $Co_3Al_4Si_2$, whose

Received: December 3, 2012
Published: February 27, 2013

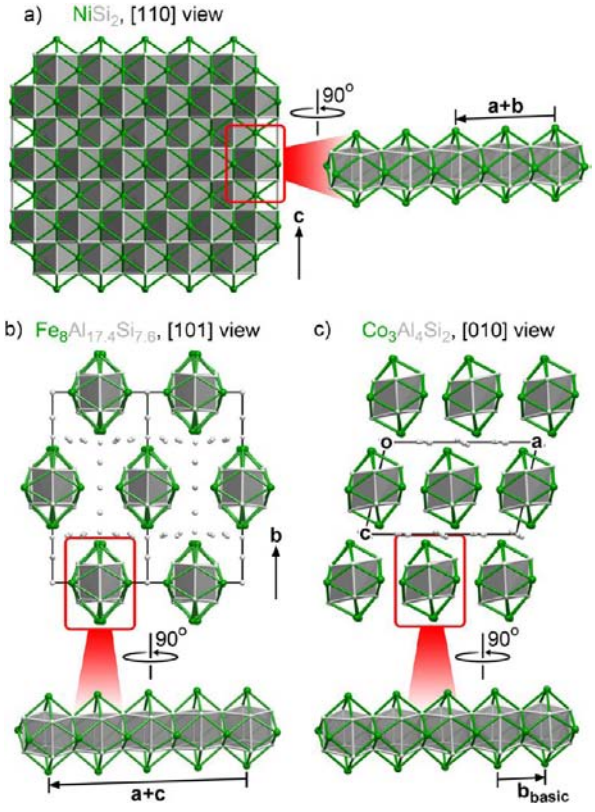

Figure 1. Structural relationships between (a) the fluorite-type $NiSi_2$, (b) $Fe_8Al_{17.4}Si_{7.6}$, and (c) the $Co_3Al_4Si_2$ phase described in this Article.

modulated structure points to an approach for incorporating such in TM−TM interactions into 18 electron bonding schemes for intermetallics.

The Co−Si−Al system has a complicated phase diagram, which is still in the process of being resolved.[11] Seven ternary phases have so far been reported,[8,12] two of which have unknown structures, including $Co_3Al_4Si_2$. Among the known structures, a variety of geometrical themes can be discerned. One is the prevalence of pentagonal columns related to decagonal quasicrystals.[12b] Another is the construction of complex structures from fragments of the fluorite type (Figure 1) as seen in $FeAl_2Si$[13] and $Fe_8Al_{17.4}Si_{7.6}$.[7]

As we will see in this paper, $Co_3Al_4Si_2$ elaborates on the latter theme. Similar to $Fe_8Si_{17.4}Si_{7.6}$, it is built from columns of the fluorite type, which are separated from each other by interfaces up to 1 atom thick. $Co_3Al_4Si_2$, however, stretches the complexity of this construction in a new dimension, into the realm of 3 + 1D superspace crystallography. The structural modulations arise from an incommensurate occupation pattern exhibited by atoms between the fluorite-type columns. Electronic calculations will show that this pattern, along with Al/Si-supported Co−Co bonding, provides the neighboring Co with the necessary coordination to adhere to the 18 electron rule. The resulting bonding scheme affirms the view of the TM−Si−Al (TM = Fe, Co, Ni) fluorite superstructures as a new class of electron phases understandable through isolobal analogies[14] to organometallic chemistry, and builds a clearer picture of how such bonding ideas may be generalized to a wider class of TM-based silicides and intermetallics.

2. TECHNICAL PROCEDURES

Synthesis. In our attempts to synthesize the two phases with unknown structures in the Co−Al−Si system, Co (Strem chemicals, 99.8%), Al (Alfa Aesar, 99.9%), and Si (Strem chemicals, 99.999%) were used as starting materials. For the synthesis of $Co_3Al_4Si_{2.3}$, the elements were weighed out in a molar Co/Al/Si ratio of 3:5:2 in an Ar-filled glovebox. The materials were then pressed into pellets and welded with an arc melting furnace on a copper hearth three times on alternating sides for optimal homogeneity. The resulting ingots were placed in the fused silica tubes under an Ar atmosphere, evacuated, and sealed. The tubes were annealed at 800 °C for 672 h (4 weeks).

Powder X-ray Diffraction Analysis. The phase purity was analyzed using powder X-ray diffraction. Each sample was ground and then poured into a 0.5 mm capillary. Data were measured on a Rigaku Rapid II diffractometer with Mo Kα radiation, λ = 0.71073 Å. Diffraction intensities were measured on an image plate detector with an exposure time of 10 min. The resulting frames were converted to intensity versus 2θ curves in steps of 0.03°. Finally, the diffraction patterns were analyzed with the programs JADE and JANA2006.[15]

Wavelength Dispersive X-ray Spectroscopy. To determine the elemental composition of $Co_3Al_4Si_2$, wavelength dispersive spectroscopy (WDS) was performed on a sample whose powder X-ray diffraction pattern showed this to be the major phase. To prepare the sample for WDS measurements, a small amount of the material was suspended in a conductive epoxy at one end of a short segment of aluminum tubing. Once the epoxy had hardened, the sample was ground down to produce a flat surface and then polished to reduce the number of surface scratches using a polycrystalline diamond suspension (Allied High Tech Products Inc., 0.25 μm) spread on a polishing wheel. As a final step, the samples were coated with 250 nm of graphitic carbon and inspected with a Cameca SX-51 electron microprobe using a voltage of 15 kV. Several choices of standards were tested. The sum of the percentages was closest to 100% when elemental Si, Al, and Co were used as standards for the respective elements.

Two phases were observed in the WDS measurements: one appearing as dark boundaries or lamellae in the SEM images, and the other as a brighter phase. The darker phase had a composition of $Co_3Al_{4.11}Si_{2.07}$ (average of 10 measurement points), which corresponds well to $Co_3Al_4Si_2$. The phase appearing brighter had a composition of $Co_{10}Al_{26.22}Si_{8.37}$ (average of 10 measurement points), which can perhaps be assigned to the phase $Co_{10.14}Al_{23}Si_{8.72}$.[11]

Single-Crystal X-ray Diffraction Measurements. Single-crystal X-ray diffraction data for $Co_3Al_4Si_2$ were collected on an Oxford Diffraction Xcalibur E diffractometer using graphite monochromatized Mo Kα radiation (λ = 0.71073 Å) at ambient temperature. Run list optimization, as well as the data processing to create a list of integrated peak intensities, the peak search, unit cell determination and refinement, the creation of reciprocal lattice reconstructions, multiscan absorption correction, and frame scaling were performed using the CrysAlis Pro v. 171.33.41 software supplied by the manufacturer. The structure was solved by the charge flipping algorithm[16] using the program SUPERFLIP,[17] and refined on F^2 using the program JANA2006.[15] Visualization of the Fourier electron density was performed with the program VESTA 3.[18] Further details regarding the crystal and the refinement are given in Table 1 and the Supporting Information.

Electronic Structure Calculations. Theoretical calculations were performed on a commensurate approximant of $Co_3Al_4Si_2$. The approximant structure was generated by beginning with the refined model and changing **q** from 0.41 $\mathbf{b}_{basic}$* to 2/5 $\mathbf{b}_{basic}$*. The 3D structure was then obtained by taking a cut perpendicular to the x_4 axis with an x_4 intercept of t_0 = 1/20, yielding a 5-fold supercell with *Cm* symmetry. Calculations of the band energies and electronic density of states curves on the commensurate approximant were performed with the Vienna Ab initio Simulation Package (VASP).[19] For these calculations, density functional theory (DFT) with the generalized gradient approximation (GGA, as implemented in the PW91 functional[20]) was employed using the projector augmented wave

dx.doi.org/10.1021/ic302650r | Inorg. Chem. 2013, 52, 3178−3189

Table 1. Crystal Data for $Co_3Al_4Si_2$

chemical formula[a]	$Co_4Al_{5.58}Si_{2.80} \approx 4/3 \times (Co_3Al_4Si_2)$[b]
WDS composition	$Co_4Al_{5.48(5)}Si_{2.75(4)}$
space group	$C2/m(0\beta0)s0$
unit cell	
a (Å)	11.8545(17)
b (Å)	3.8805(6)
c (Å)	7.4309(11)
β (deg)	103.091(15)
q	~0.41 **b***
cell volume	334.59(16)
Z	2
cryst. dimensions (mm^3)	0.06 × 0.08 × 0.10
crystal color	metallic black
crystal habit	irregular
data collection temp.	RT
radiation source, λ (Å)	Mo, Kα (0.7107)
absorption coef. (mm^{-1})	10.925
absorption correction	multiscan
θ_{min}, θ_{max}	3.53, 28.59
number of reflns	10 379
refinement method	F^2
R_{int} [all, $I > 3\sigma(I)$]	4.44, 3.38
number of params	159
all reflections	
unique reflns. ($I > 3\sigma$, all)	733, 2061
$R(I > 3\sigma)$, $R_w(I > 3\sigma)$	2.50, 4.26
R(all), R_w(all)	8.69, 5.10
main reflections	
unique reflns. ($I > 3\sigma$, all)	371, 460
$R(I > 3\sigma)$, $R_w(I > 3\sigma)$	1.86, 4.32
R(all), R_w(all)	2.51, 4.36
satellites, m = 1	
unique reflns. ($I > 3\sigma$, all)	291, 807
$R(I > 3\sigma)$, $R_w(I > 3\sigma)$	4.24, 7.36
R(all), R_w(all)	14.04, 9.35
satellites, m = 2	
unique reflns. ($I > 3\sigma$, all)	71, 794
$R(I > 3\sigma)$, $R_w(I > 3\sigma)$	9.71, 20.04
R(all), R_w(all)	37.19, 31.25
$S[I > 3\sigma(I)]$, S(all)	1.69, 1.02
$\Delta\rho_{max}$, $\Delta\rho_{min}$ ($e^-/Å^3$)	0.77, −0.84

[a]See text for details of determination of the chemical formula. [b]For simplicity we will refer to the compound according to its historical name "$Co_3Al_4Si_2$", even though this is not the simplest representation of the unit cell contents.

potentials[21] supplied with the program. The calculations were carried out in the high-precision mode (corresponding to an energy cutoff of 335.0 eV), using a Γ-centered 3 × 3 × 5 k-point grid. Projected DOS curves were calculated using the procedure described in the VASP manual: the portions of the wave functions occurring inside fixed spheres surrounding the ion positions were projected onto spherical harmonics to obtain the s-, p-, and d-type contributions for each atom. The sphere radii were chosen such that the sum of the sphere volumes equaled the total unit cell volume, while the ratios of the radii conformed to those of the atomic radii (as given by the Wigner−Seitz radii in the potential files).

Once the GGA-DFT band energies and DOS curves were obtained, they were used as a basis for the parametrization of a Hückel model for the structure. The Hückel parameters were refined using the eHtuner program,[22] obtaining a root-mean-squared deviation of 0.089 eV for the bands up to 2 eV above the Fermi energy (E_F). Hückel calculations were carried out using the YAeHMOP program,[23] and the Hamiltonian matrices were output for further processing using custom-made MATLAB scripts.

3. THE CRYSTAL STRUCTURE OF $Co_3Al_4Si_2$

Preliminary Examination of Crystals. The crystals picked from the $Co_3Al_4Si_2$ samples were invariably multiply twinned. Fortunately, the random orientations of the twin lattices generally led to minimal overlap between the reflections of the lattices, making structure determination possible. The best specimen examined exhibited at least three twin domains with a C-centered monoclinic unit cell, a = 11.85 Å, b = 3.88 Å, c = 7.43 Å, β = 103.1°, matching that previously reported for $Co_3Al_4Si_2$.

Inspection of reciprocal lattice reconstructions, however, revealed that this is not the full story (Figure 2). Satellite peaks

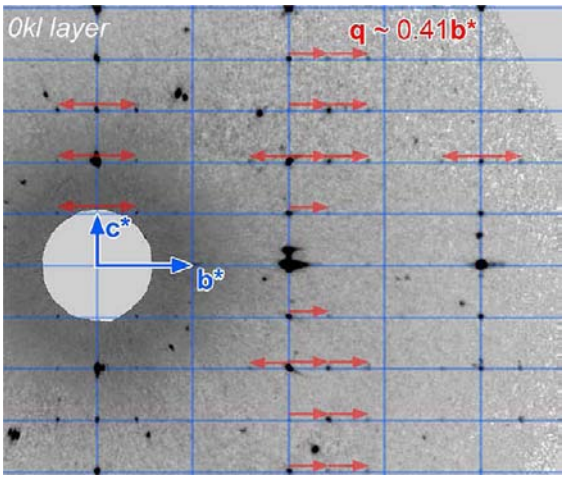

Figure 2. Reconstruction of the 0kl reciprocal lattice layer of $Co_3Al_4Si_2$ from a single-crystal X-ray diffraction data. The C-centered orthorhombic basic cell is indicated with a blue grid, while a selection of satellites are indicated with red arrows. Because of the multiply twinned nature of the sample, a number of spurious spots are also apparent.

are observed stemming from the indexed reflections along the b* direction, corresponding to a **q** vector of approximately 0.41 **b***. This indicates that the compound adopts a modulated structure. The **q** value of ~0.41 could be interpreted as any of several rational numbers, such as 2/5 and 5/11, both of which are within the experimental uncertainty of our determination of **q**. These values of 2/5 and 5/11 would correspond, respectively, to a 5-fold and 11-fold superstructure along the b direction. Such ambiguity in the unit cell parameters would be quite unsettling for a conventional structure refinement. For this reason, the assumption that the phase is incommensurately modulated, using the 3 + 1D superspace formalism, provides a more meaningful avenue to structure determination.[24]

The Average Cell. As a starting point to determining the full modulated structure of $Co_3Al_4Si_2$, it is helpful to begin with the main reflections and solve the structure of the basic cell. The details of the point symmetry of the diffraction pattern and systematic absences are consistent with the space group $C2/m$ (or a subgroup of it) for this cell. Attempts at structural solution using the basic cell reflections in space group $C2/m$ yielded the composition $Co(Al/Si)_{2.09}$. This was initially solved with all Al atoms on the Al/Si positions. Through an analysis of the interatomic distances (see Figure S5 of the Supporting

dx.doi.org/10.1021/ic302650r | Inorg. Chem. 2013, 52, 3178−3189

Information), it was eventually possible to tentatively assign some of these sites to Al or Si based on their distances to Co atoms being relatively long or short, respectively. In the case of one ambiguous site, labeled as Si3, a mixed occupancy was assigned so that the structure's Al/Si ratio matched that of the WDS result.

The resulting structure, presented in Figure 3, bears similarities of $Fe_8Al_{17.4}Si_{7.6}$ (Figure 1b). As with $Fe_8Al_{17.4}Si_{7.6}$,

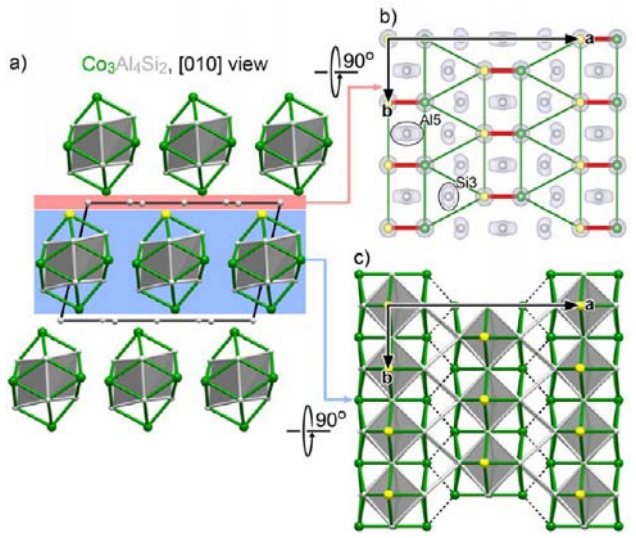

Figure 3. Crystal structure of the average cell of $Co_3Al_4Si_2$. A [010] view is given in (a) with slabs corresponding to interstitial layers and fluorite-type columns highlighted in red and blue, respectively. These slabs are laid out in (b) and (c). In (b), yellow and green spheres represent Co atoms occurring above and below the Al/Si atoms (gray). An isosurface of the Fourier electron density (at 5.0 electrons/Å^3) in the interstitial layer is also shown to illustrate the nonspherical features surrounding the Si3 and Al5 sites.

the structure is based on a rod packing of fluorite-type columns, each consisting of a strip of edge-sharing Si/Al cubes whose square faces are capped by TM atoms. The columns meet each other at two types of interfaces: edge-to-edge and face-to-face interfaces across which, respectively, the Si/Al cube edges and faces meet.

As in $Fe_8Al_{17.4}Si_{7.6}$, the edge-to-edge interfaces are structured so that the cubic Si/Al network passes continuously from one fluorite column to the next (Figure 3c). Unlike $Fe_8Al_{17.4}Si_{7.6}$, however, no additional atoms are present buffering the columns from each other. The columns are shifted relative to each other along b such that the Si/Al cube edges of one column face the inner, shared cube edges of the neighboring one to form new cubes. The nascent cubes are all filled with Co atoms from the participating fluorite-type columns. These cubes share faces (as in the CsCl type) to form a zigzag chain, giving each Co atom two Co neighbors from across the cube faces for a total coordination of 8 Si/Al + 2 Co atoms.

At the face-to-face interface (Figure 3b), a layer of interstitial Al/Si atoms occurs in the spaces between the TM atoms, but problems evidently are encountered in finding a suitable periodic pattern. Isosurfaces of the Fourier electron density for this portion of the structure do not show the spheres expected for well-defined atomic positions. Elongated shapes are present—bean-shaped surfaces in the triangular holes formed by the Co atoms above and below, kinked rods in the rectangular ones—indicative of disorder.

From this analysis of the average cell of $Co_3Al_4Si_2$, it is apparent that the positions of the Si/Al atoms at the face-to-face interface layer are not well-located within the constraints of a simple periodic structure. We might then expect that the satellite reflections in the diffraction pattern of this phase (Figure 2) may emerge from an incommensurate placement of the atoms within this layer. In the next two sections of this Article, we will explore this possibility with a refinement of the full modulated structure of $Co_3Al_4Si_2$.

Moving to 3 + 1D Space. The 3 + 1D superspace formalism for incommensurately modulated phases provides a way to solve and refine the structural features underlying $Co_3Al_4Si_2$'s satellite reflections, and also to describe them in terms of a handful of meaningful structural parameters. In this approach, we recognize that in moving down the incommensurate direction of the structure, y, we are actually following two periodicities: that of the basic cell (repeat vector = $\mathbf{b}_{basic}$), and that of the modulation function acting on the basic cell (repeat vector = λ). An atom's position along the y axis can then be expressed either with respect to the basic cell ($x_2 = y/b_{basic}$) or with respect to the modulation wave ($x_4 = y/\lambda$). In this way, an atom's coordinate in physical space (x, y, z) becomes mapped onto a point (x_1, x_2, x_3, x_4) in an abstract 3 + 1D space. The elegance of this construction lies in the feature that all of the axes are periodic, and a unit cell—the prerequisite for any crystallographic analysis—is obtained from what in physical space is aperiodic.

When we index the reflections in the diffraction pattern as $\mathbf{G} = h\mathbf{a}^* + k\mathbf{b}^* + l\mathbf{c}^* + m\mathbf{q}$, the four reciprocal basis vectors correspond to the $\mathbf{a}_1$, $\mathbf{a}_2$, $\mathbf{a}_3$, and $\mathbf{a}_4$ cell vectors of the 3 + 1D unit cell. The contents of the 3 + 1D unit cell can then be solved and refined just as in a simple 3D structure. Finally, the physical structure in 3D is recovered by making a cross section of the 3 + 1D space such that the correct relationships of y to x_2 and x_4 are obeyed: $\mathbf{r} = x_1\mathbf{a}_1 + x_2\mathbf{a}_2 + x_3\mathbf{a}_3 + qx_2\mathbf{a}_4 = x\mathbf{a} + y\mathbf{b}_{basic} + z\mathbf{c}$.

The first step in applying this approach to $Co_3Al_4Si_2$ is the determination of the 3 + 1D superspace group within which the higher-dimensional model of this phase should be built. As is described in detail in the Supporting Information, the point symmetry of the diffraction pattern and systematic absences lead us to the superspace group $C2/m(0\beta0)s0$. In this nomenclature, the $C2/m$ component indicates that the 3 + 1D symmetry operations are derived from this 3D space group. Next, the "$(0\beta0)$" tells us that the $\mathbf{q}$ vector is parallel to $\mathbf{b}^*$. Finally, the "s" and "0" indicate whether the 2-fold axes and mirror planes, respectively, of the $C2/m$ space group have acquired an x_4 glide on moving to 3 + 1D space. "s" denotes a glide of 1/2, while "0" means that no glide is associated with the specific symmetry operation. The choice of this 3 + 1D space group was confirmed by Jana2006's superspace group test and the successful structure solution and refinement of the $Co_3Al_4Si_2$ structure, as we will describe presently.

The Modulated Structure of $Co_3Al_4Si_2$. Now that we have identified the 3 + 1D superspace group for $Co_3Al_4Si_2$, structure solution becomes possible using the charge-flipping algorithm,[16] as is implemented in the program SUPERFLIP.[17] This method for determining the electron density distribution from a diffraction pattern has the advantage that it is dimension-independent, making it applicable to structures modeled in superspaces or higher-D spaces. It also makes no assumptions about the symmetry of a structure, and the

dx.doi.org/10.1021/ic302650r | Inorg. Chem. 2013, 52, 3178−3189

symmetrization process of the final electron density distribution provides an independent check on our space group choice.

Upon applying the charge-flipping algorithm to our single-crystal X-ray diffraction data set for $Co_3Al_4Si_2$, SUPERFLIP quickly converged on a 3 + 1D electron density that obeyed well the symmetry operations of our chosen space group $C2/m(0\beta0)s0$. Preliminary atomic positions were then extracted using the Jana2006's peak-search utility. From inspection of the electron density maps surrounding the atomic positions, improvements to the model were made where the initial assignments of the Jana2006 program did not suffice. Refinement of the model against the diffraction data, as well as the inclusion of modulated anisotropic atomic displacement parameters, led to an overall R-factor for all observed reflections ($I < 3\sigma$) of 2.50. This corresponded to R-factor values for the main reflections, first-order satellites, and second-order satellites of 1.86, 4.24, and 9.71, respectively (see Table 1 for further details of the refinements).

In our refinement of the basic cell structure of $Co_3Al_4Si_2$, we observed smeared electron density features at the Si/Al atoms in the face-to-face interface layer. Not surprisingly, the modulations giving rise to the satellite reflections are largely localized to these Al/Si positions, Si3 and Al5 (see Tables S2 and S3 in the Supporting Information for coordinates, ADP parameters, and modulation amplitudes, as well as a discussion of the relatively high U_{equiv} values for these strongly modulated positions).

The Si3 position appears to be the dominant factor in driving the modulation. In Figure 4a, we illustrate the modulation of this position with a cross section of the 3 + 1D space showing how the x_2-coordinate of this atom varies as a function of the modulation wave phase (x_4). Solid gray lines give our structural model's positions for Si3, while thin black curves trace out contours of the Fourier electron density for comparison. The Si3 atomic domains appear as slanted line segments centered on the positions (x_2, x_4) = (0.0, 0.75) and (0.5, 0.25), as well as their translationally equivalent points.

Following any such domain along the x_4 axis shows how the atom's position changes with the phase of the modulation function. For instance, if we start at the point x_2 = 1.0, x_4 = 0.0 and move vertically up the figure, we see that, at first, the atomic position is vacant; then, at about x_4 = 0.5, an atom appears shifted to the $+x_2$ side of the average Si3 position of x_2 = 1.0. The atomic position then drifts gradually to the $-x_2$ side of x_2 = 1.0, until it disappears at about x_4 = 1.0, only to reappear at the $x_4 \sim 1.5$ at the $+x_2$ side again. This zigzag pattern then repeats along the x_4 axis.

In looking at the distribution of the Si3 atomic domains in Figure 4a, one may be struck by how the continuities between domains along the x_4 direction are not nearly as strong as those neighboring each other along x_2. This is highlighted by the contours, which trace out slightly kinked stripes of electron density running diagonally down the map. The occurrence of such slanted atomic domains is the hallmark of a specific class of modulated structures: composite structures, in which incommensurability arises from the coexistence of two sublattices of differing periodicity.[24b,25] The slanted domains allow for those atoms to be sampled at a different frequency by physical space (as obtained by taking a 3D cross section of the 3 + 1D model perpendicular to the x_4 axis) than those atomic domains aligned with x_4.

On the basis of this observation, we might conclude that the incommensurate structure of $Co_3Al_4Si_2$ stems from the Si3

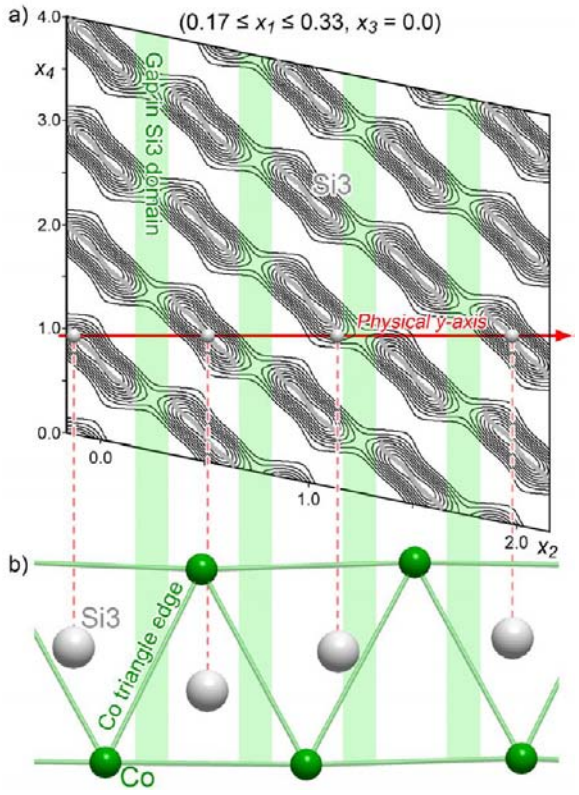

Figure 4. Si3 atomic domains in the 3 + 1D model of $Co_3Al_4Si_2$, and the corresponding atomic positions in physical space. (a) A (x_2, x_4) plane of the 3 + 1D model taken through Si3 positions. To capture the full extent of the Si3 domains along x, a layer thickness of 2 Å was used along x_1. The crystallographic model's Si3 positions are given with thick gray curves, with contours of the Fourier electron density (summed over the layer thickness along x_1) shown for comparison in thin black lines. (b) The Si3 positions obtained from a cross section of the 3 + 1D model perpendicular to the x_4 axis. Pale green bars show the coincidence of the Si3 domain gaps in (a) and the centers of the Co−Co triangle edges in the Si3 coordination environments.

atoms adopting a different spacing along the y axis than the other atoms in the crystal. As we will see below, this is largely borne out in the images of the incommensurate structure in physical space. One difference from a traditional composite structure, however, is notable: moving along any of the slanted stripes of Figure 5a shows that the electron density is not uniformly distributed. The density drops significantly at the kinks that separate the Si3 domains.

These dips in the electron density seem to correspond to forbidden regions where Si3 atoms are not found. These gaps along the y axis can be understood by considering the structural context in which the Si3 atoms exist. As was described above, each Si3 position lies at the center of a triangle of Co atoms. The Co triangles share edges to form strips running along y. If we align one such strip with the (x_2, x_4) map, as in Figure 4b, a correlation becomes apparent. As is highlighted with light green bars, the gaps in the Si3 electron density in the 3 + 1D model coincide with edges of the Co triangles in physical space. The placement of Al/Si atoms at these positions would then cause a drastic change in their coordination relative to the triangle centers: rather than capping a Co triangle, these Al/Si atoms would bridge a pair of Co atoms. The resulting Co−Al/Si distances would be unusually short, about 2.19 Å. The gaps in the slanted rows of electron density in Figure 4a indicate that

dx.doi.org/10.1021/ic302650r | Inorg. Chem. 2013, 52, 3178−3189

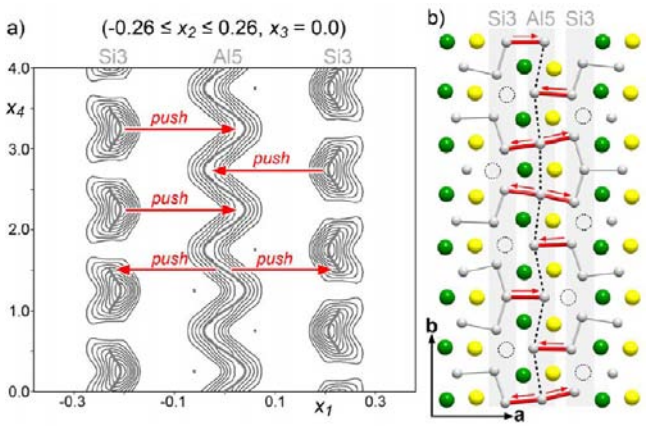

Figure 5. Positional correlations in the modulations of the Si3 and Al5 positions. (a) Map of the 3 + 1D Fourier electron density centered on the Al5 position and summed over 2.0 Å along x_2. The crystallographic model's positions for the Si3 and Al5 sites are drawn for comparison with thick gray curves. Horizontal cuts correspond roughly to atomic positions simultaneously occupied. When only one of the two Si3 sites surrounding the Al5 is occupied, the Al5 site tends to move into the vacant space. When both Si3 sites are occupied, they both move to avoid the Al5 atom. (b) The resulting pattern in physical space.

such geometries are unfavorable. Although the distribution of Si3 sites is incommensurate with $\mathbf{b}_{basic}$, it is not entirely independent.

In summary, the Si3 sites are arranged along the y axis with a spacing that is incommensurate with that of the basic cell of Co_3AlSi_2. Simple occupation of the Co triangles would lead to two Si3 atoms per $\mathbf{b}_{basic}$ repeat. Instead, the slanting of the Si3 domains reduces the frequency with which the physical y axis crosses the Si3 domains to about 1.41 times per unit cell (see section S2 of the Supporting Information), such that the average spacing between Si3 atoms along y ($\mathbf{b}_{Si3}$) would be 0.71 $\mathbf{b}_{basic}$. The presence of forbidden positions at the triangle edges drops the number of Al atoms per $\mathbf{b}_{basic}$ repeat further to 1.38. The average presence of 1.38 atoms on the two available Si3 sites in the basic cell corresponds to an average occupancy of 0.69, which is in reasonable agreement with that value of 0.66 obtained in the refinement of the basic cell.

The incommensurate placement of the Si3 atoms in $Co_3Al_4Si_2$ thus appears to be the major geometrical factor underlying the modulations of this structure. The remainder of the modulation functions can be envisioned as responses to this Si3 occupation pattern. The diffuse electron density features of the Al5 sites in the basic cell refinement suggest that this site is most strongly affected by the Si3 pattern. As in the basic cell, the shortest Si3−Al5 contacts occur along the x direction; the most direct way to examine their interactions is by examining how the Al5 x_1-coordinates change as a function of x_4 (and thus the presence or absence of the Si3 atom). This is illustrated in Figure 5a. Here, contours are shown of the Fourier electron density summed over a range in x_2 to capture both the Si3 and the Al5 atoms. The model's positions for Si3 and Al5 are traced with gray curves.

The Si3 positions in this plot appear as discrete arc-shaped domains occurring at about $x_1 = -0.25$ and +0.25, respectively. The presence of the Si3 atoms at these two x_1 values is staggered so that the center of one Si3 domain at $x_1 = -0.25$ occurs at the gap between those domains at $x_1 = 0.25$ and vice versa. Such staggering is reminiscent of glide or screw operations, and indeed, it arises from the $(x_1, x_2, x_3, x_4) \rightarrow (-x_1, x_2, -x_3, x_4 + 1/2)$ operation of the space group $C2/m(0\beta0)s0$.

The atomic domain for Al5 is centered between the two Si3 positions along the x axis at $x_1 = 0$ and exhibits a strong sinusoidal shape. Comparison of the positions of the maxima and minima of the Al5 curve with the locations of the Si3 domains reveals that the two types of features are closely correlated. The Al5 curve's extrema are directed away from Si3 domains and toward the gaps between them. As the Si3 domains are staggered between $x_1 = \pm0.25$, this results in the Al5 curve oscillating with the same period.

The out-of-phase character of the Al5 oscillations and the Si3 occupation pattern hints that the interactions between these sites are repulsive, as is highlighted with red arrows in Figure 5a. This hypothesis provides an explanation for the curved shape of the Si3 domains. The tips of these domains coincide in physical space with the inflection points in the Al5 curve. At these points along the x_4 axis, a transition is occurring between the occupation of one Si3 position and its symmetry-related partner on the other side of the Al5 curve. Here, there is a small range in x_4 in which Si3 atoms are present on both sides of the Al5 atom. Situtated between the two Si3 atoms, the Al5 cannot move to avoid them. Instead, the Si3 atoms move away to make room.

Figure 5b shows how this Si3−Al5 interaction plays out in physical space with a view of the interstitial layer of atoms at the face-to-face interfaces between fluorite-type columns (cf. Figures 3b and 4b). The Si3 and Al5 atoms are highlighted with vertical gray columns running along the strips of edge-sharing Co triangles and rectangles, respectively. Some gaps occur in the occupation of the Co triangles by Si3 atoms, and at such positions, the nearest Al5 site migrates slightly toward the vacancy as though pushed by the Si3 atom on the opposite side. Where Si3 atoms occur on both sides of an Al5 atom, the Al5 atom stays close to the middle of its Co rectangle, and the Si3 atoms are displaced instead.

The Si3 and Al5 sites we have just discussed exhibit the most pronounced modulations in the structure of $Co_3Al_4Si_2$. Harmonic modulation waves were also refined for the remaining atoms, but these were found to have much more minor amplitudes. The values of all modulation parameters used in the refinement are listed in Table S3 of the Supporting Information.

In this section, we have seen that the satellite reflections observed in the diffraction pattern of $Co_3Al_4Si_2$ correspond to an incommensurate ordering of the Si/Al atoms at the face-to-face interfaces. The Si3 atoms form chains along the y axis with a spacing that is largely independent of the basic cell, while the Al5 position wobbles back-and-forth in response. Having determined the nature of these modulations, we may now wonder in what way this incommensurability contributes to the stability of $Co_3Al_4Si_2$. It is with this question in mind that we now turn to the electronic structure of $Co_3Al_4Si_2$.

4. THE ELECTRONIC STRUCTURE OF $Co_3Al_4Si_2$

An Approximant Structure for Theoretical Analysis. Given the predominance of electronic stabilization in transition-metal silicides and aluminides, we began our investigation into the bonding in $Co_3Al_4Si_2$ with GGA-DFT calculations of its electronic DOS distribution. Several factors make some simplifications of the $Co_3Al_4Si_2$ structure necessary for a GGA-DFT approach to be feasible. The most obvious is

dx.doi.org/10.1021/ic302650r | Inorg. Chem. 2013, 52, 3178−3189

the incommensurability along the b axis of the structure. Another challenge is the modeling of the mixed Al/Si sites in the crystallographic model.

In our calculations, we addressed these issues with the following simplifications: (1) We approximated the q-vector $\mathbf{q}$ = 0.41 $\mathbf{b}_{basic}$* as 0.40 $\mathbf{b}_{basic}$* = 2/5 $\mathbf{b}_{basic}$*, thus creating a periodic 5-fold superstructure of the basic cell. (2) The Al/Si ratios of the mixed sites were rounded to the nearest integer. Together, these modifications yielded a structure with *Cm* symmetry and a composition of $Co_3Al_{3.8}Si_{2.6}$, which is relatively Si-rich compared to the experimental formula, $Co_3Al_{4.2}Si_{2.1}$. While at first glance, this may seem to be a large change in Si content of the phase, the overall change to the electron concentration is only from 15.99 electrons/Co (experimental) to 16.15 electrons/Co, that is, less than 0.2 electrons/Co atom.

Even with these approximations, we will see that these DFT calculations form the basis for a robust description of the bonding in this phase, one that stems more from orbital symmetry than from a specific q-vector or composition.

DOS Pseudogap Stabilization of $Co_3Al_4Si_2$. The resulting GGA-DFT DOS distribution is plotted in Figure 6a.

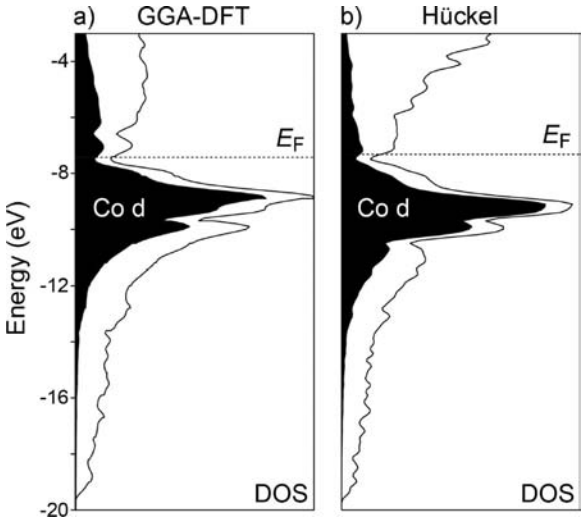

Figure 6. Electronic DOS distribution of a simplified version of $Co_3Al_4Si_2$ calculated using (a) GGA-DFT and (b) a DFT-calibrated Hückel model. Contributions to the DOS from the Co d orbitals are shaded. See text for a description of the structural approximations taken to make the calculations feasible.

As in other TM−main group compounds, the predominant feature of the DOS distribution is a mountain-like peak of states corresponding to the TM d orbitals. Below this peak is a long, parabolic tail rich in Al/Si sp character. The Fermi energy (E_F) lies just above the Co d peak at about −7.3 eV, and lies in a narrow DOS minimum. While the DOS value here is substantially larger than the value of zero needed for a bona fide band gap, the coincidence of the E_F both with this minimum and an essentially filled Co 3d block suggests that a stable electron configuration has been achieved.

Similar DOS features were found for the structurally related compound $Fe_8Al_{17.4}Si_{7.6}$, which is also constructed from columns of the fluorite type. In $Fe_8Al_{17.4}Si_{7.6}$, the DOS pseudogap at the E_F had a simple explanation: the coordination environments of the Fe atoms exhibited molecular orbital diagrams analogous to 18 electron complexes. To see if a similar scheme could be at work in $Co_3Al_4Si_2$, we refined a best-fit Hückel model[22] against the DFT band energies and DOS curves, translating the DFT results into an effective orbital-based picture.

The $Co_3Al_4Si_2$ DOS curve for the resulting Hückel model is presented alongside that from DFT in Figure 6b. While some differences occur between the curves, particularly above the E_F, the Hückel model reproduces key features of the DFT electronic structure: the position, depth, and width of the DOS pseudogap near the E_F, as well as the overall form of the distribution below the pseudogap. On the basis of these correspondences, we will proceed with analyzing the Hückel model in place of the full DFT results.

Electron Counting in the Co2 Dimers. In our earlier bonding analysis of $Fe_8Al_{17.4}Si_{7.6}$ and the parent fluorite type, as exemplified by $NiSi_2$, we saw that a productive starting point was to consider simple MO models in which the transition-metal atoms are coordinated by σ orbitals from their surrounding Si/Al atoms. For $Co_3Al_4Si_2$, we are emboldened to pursue such an approach by the location of the E_F just above a broad peak of Co d states, with its suggestion of a nearly closed-shell electron configuration on the Co atoms. In the next two sections, we will see that this path indeed leads to an explanation for the DOS pseudogap of $Co_3Al_4Si_2$. As before, the bonding scheme will stem from the 18 electron rule. This time, however, a new feature will come to the foreground: the covalent sharing of electrons between Co atoms.

Two symmetry-distinct atomic domains for Co are present in the 3 + 1D model for this structure: Co1 and Co2. The Co1 sites trace out zigzag chains along the edge-to-edge interface between fluorite-type columns (black dashed lines in Figure 3c), with Co−Co distances of about 2.61 Å. Of all atoms in the structure, these sites are furthest from the face-to-face layers where the structural modulation is most pronounced; the closest atom in the interstitial layer to any given Co1 atom is greater than 3.7 Å. We will consider these atoms as being largely unaffected by the modulation, and derive our MO model for this site from the basic cell.

The Co2 atomic domain, however, corresponds to the Co atoms that occur at the face-to-face interface. As this is the region where the modulation is strongest, the coordination environment changes dramatically as the 3D crystal structure crosses the Co2 domain at different points along the x_4 axis. At all points along the x_4, however, the Co2 atoms occur as pairs, with a Co−Co distance of ca. 2.67 Å. In our commensurate approximant, dimers occur with five distinct values of x_4.

The Co1 and Co2 sites then correspond to two fundamentally different motifs in the structure: Co chains and Co dimers, both of which occur in a context of Si/Al neighbors. Because of their greater simplicity, we will start with the Co2 dimers. The Co−Co distances in the Co2 dimers (about 2.67 Å) are sufficiently close to that in elemental Co (2.5 Å[26]) that the potential for interaction along this contact cannot be ignored. For this reason, we will consider pairs of Co atoms coordinated by their near Si/Al neighbors in our MO models, rather than individual Co atoms. On each Si/Al neighbor, we place an sp^2-hybridized σ orbital directed toward either the closed Co atom (for atoms in contact with only one of the two Co atoms) or the center of the Co−Co contact (for atoms bridging the Co−Co dimer). It is also important to include in the basis set a p orbital on each of the bridging Si/Al atoms running parallel to the Co−Co contact.

In Figure 7a, we display the MO energies for the Co2 clusters created for the five different values of x_4 encountered in our

dx.doi.org/10.1021/ic302650r | Inorg. Chem. 2013, 52, 3178−3189

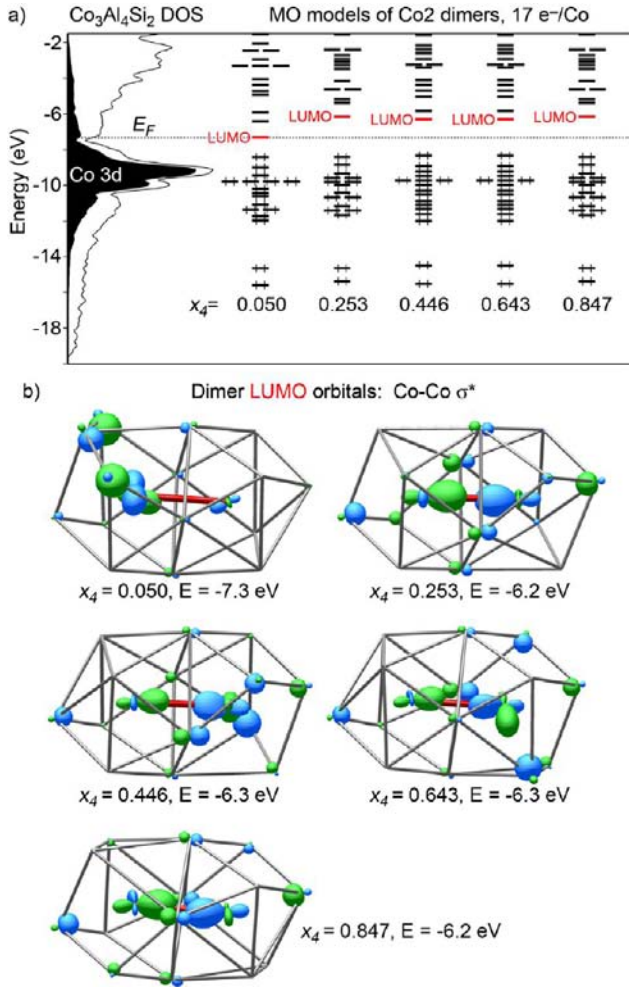

Figure 7. Bonding analysis of the Co2 sites in $Co_3Al_4Si_2$. (a) Hückel molecular orbital energy levels for cluster models of the Co2 dimers occurring in the commensurate model of the structure, drawn alongside the DOS distribution for the full compound. (b) Plots of the lowest unoccupied molecular orbitals (LUMOs) of the clusters in (a). At 17 electrons/Co, the LUMO level is Co−Co σ antibonding, indicating that an 18 electron configuration on each Co atom is achieved through the covalent sharing of an electron pair.

approximant structure. All five diagrams show a similar distribution of energy levels: two low levels occur just below −14 eV, followed by a dense block of states ranging from about −12 to −8 eV. After this, a gap occurs (of about 2 eV in all but x_4 = 0.05), and finally, a series of closely spaced high-lying levels are present. The conspicuous energy gap between the middle and high-energy blocks corresponds to a filling of 34 electrons, or 17 electrons per Co atom.

These features coincide in energy well with features in the DOS curve for the full compound (Figure 7a, right). The pair of low-lying levels lies near the center of the parabolic sp distribution at the low end of the DOS curve. The middle energy block of MO levels spans about the same range as the Co 3d peaks in the DOS, while the high-energy block coincides with the large DOS values above the E_F. Most importantly, the HOMO−LUMO gaps for the molecular clusters all straddle the DOS pseudogap for $Co_3Al_4Si_2$. The HOMO−LUMO gaps in the clusters at 17 electrons/Co atom thus provide a good model for the Co2 contributions to the pseudogap.

The count of 17 electrons/Co atom is one electron short of that expected by the simple 18 electron rule. Yet, the large HOMO−LUMO gaps occurring for this electron count suggest that a stable configuration has been achieved. This can be understood by examining the lowest unoccupied molecular orbitals (LUMOs) for these clusters, as are displayed in Figure 7b. In all but the x_4 = 0.05 orbital (which has the smallest HOMO−LUMO gap), the LUMOs are dominated by large lobes on the Co atoms directed at each other. These lobes are out-of-phase and contribute a strong Co−Co σ antibonding character to the orbital.

The presence of these Co−Co σ* orbitals above the HOMO−LUMO gap hints that occupied Co−Co σ bonding levels should also be present. Indeed, for each of the clusters, one of the two lowest-lying levels is based on a Co−Co σ bonding orbital with stabilizing contributions from the surrounding Si/Al atoms (Figure 8). In the 34-electron clusters,

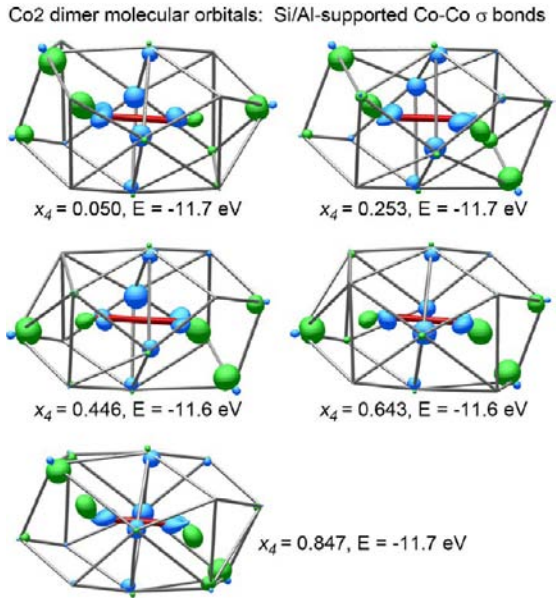

Figure 8. Occupied molecular orbitals of the model Co2 dimer clusters exhibiting Co−Co σ interactions supported by bridging Si/Al atoms. The nodal character of the multiorbital overlap centered on each Co−Co contact allows for an isolobal analogy to a classical two-center two-electron σ bond.

then, it appears that one MO contains an electron pair that is shared between the two Co atoms in a covalent sense. Through this sharing of an electron pair, the 17 electrons per Co allows for a full 18 electron configuration on each Co atom.

Does this mean that direct Co−Co bonds exist in $Co_3Al_4Si_2$? A calculation on an isolated pair of Co atoms (not shown) suggests that this is not the case. At a distance of 2.67 Å, the Co−Co σ interaction does not produce an energy dispersion at all approximating that seen in Figure 7a. Instead, the energy difference between the nominally Co−Co σ and σ* levels appears to be largely determined by the different degrees to which they can be stabilized by σ orbitals on the bridging atoms. For the Co−Co σ orbital, the in-phase combination of Co orbitals allows for a strong interaction with the sp^2-hybrid orbitals on the bridging Si/Al atoms. In the case of the Co−Co σ* orbital, however, the sp^2-hybrids on the bridging atoms would point along a nodal plane, leading to no net overlap. Instead, the Co−Co σ* orbital is stabilized via the tangential p

dx.doi.org/10.1021/ic302650r | Inorg. Chem. 2013, 52, 3178−3189

orbitals on the bridging atom, which is evidently not sufficient for pushing the level below the HOMO−LUMO gap.

The covalently shared electron pair should thus be envisioned as belonging to a multicenter bonding orbital that has the nodal character of a Co−Co σ-bond. We can thus view the bonding situation as isolobal[14] to a true Co−Co σ bond, while recognizing the key role of the bridging orbitals. In this way, the electron counting proceeds in the same way as TM metal complexes with TM−TM bonding. As we will see below, this approach also proves useful in understanding the bonding along the Co chains defined by the Co1 atomic domains.

The Band Structure of the Co1 Chains. We now turn to the chemical bonding at the second set of Co atoms in the structure, the Co1 sites. These sites show structural similarities to those of Co2, similarities that will be reflected in the electronics. As in the Co2 dimers, the Co1 atoms meet each other across square faces of Si/Al atoms. This time, two such Co−Co contacts occur to each Co1 atom, leading to zigzag chains. The Co−Co distances here of 2.61 Å are again too short for the coordination environments of the Co to be considered individually. Instead, we must consider the Co1 chain as a whole.

To do this, we imagine a hypothetical 1-D periodic system based on a strand of Co1 atoms, and their immediate nearest neighbors, as is shown in Figure 9a. To focus on the bonding

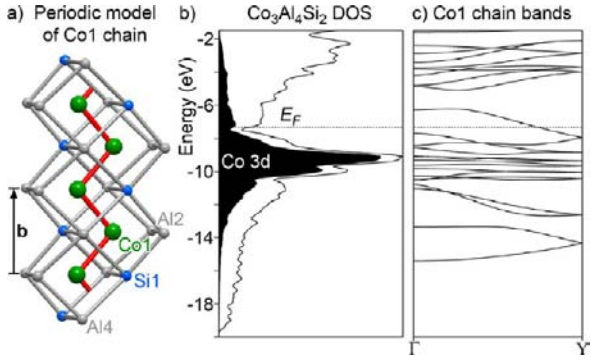

Figure 9. Band structure for a 1D periodic model of the Co1 coordination environment and the full DFT-calibrated Hückel DOS curve of $Co_3Al_4Si_2$. (a) The atomic positions in the periodic model. (b) The DOS curve for a periodic approximant to $Co_3Al_4Si_2$ (see Figure 6b). (c) The band structure for the Co1 chain. The Fermi energy (E_F) for the full DOS calculation crosses a single band in the Co1 chain model. See text for details of basis used in the calculation of (c).

experienced by the Co atoms, we place on each Si/Al atom an sp^2 hybrid orbital pointing to the nearest Co atom(s), and for those that are bridging Co−Co contacts, we also provide a p orbital directed along the axis of the chain.

Because this is an extended system, the results of the DFT-calibrated Hückel calculation appear as a band structure rather than an MO diagram containing discrete energy levels.[27] The band structure obtained is shown in Figure 9c. On moving from the bottom of the energy axis upward, we first encounter a couple of disperse bands at −16 to −13 eV. Next, is a tight bundle of narrow bands from about −12 to −8 eV. This is followed by an opening, across which a lone band is stretched, and finally a group of high-lying bands.

As we saw for the MO diagrams for the Co2 dimers, there are correspondences between this Co1 band structure and the full DOS curve of the $Co_3Al_4Si_2$ structure (Figure 9b). The low-energy disperse bands, the bundle of narrow bands at intermediate energy, and the high-lying block of bands, coincide well with, respectively, the parabolic sp region, the d block, and the unoccupied states in the DOS distribution. Most importantly, the opening in the band structure of the Co1 chain at about −7 eV aligns almost exactly with the DOS pseudogap at the E_F for the full compound.

We can now go deeper into interactions leading to the DOS pseudogap. The opening of the band structure near the $Co_3Al_4Si_2$ E_F occurs after 15 bands are fully occupied. As there are two Co atoms/cell of the zigzag chain, this corresponds to 15 electrons per Co, well below the 18 electrons expected for isolated TM atoms.

The covalent sharing of electrons at the Co−Co contacts could reconcile this difference. The main difficulty in testing the hypothesis of Co−Co shared electron pairs is identifying the involved orbitals in the band structure. A simple way to locate the relevant bands is through a fat-band analysis, in which the thickness of the curves in the band structure is weighted by the contribution from specific orbitals. In Figure 10a, we plot the Co1 chain band structure again, this time with the contributions from the Co s and σ-oriented p orbitals highlighted with red curves. The Co sp contributions appear very strong in the lowest band as it rises in energy from Γ (k = 0) to Y ($k = \pi/b$). At the Y k-point, this σ band bends back and then passes upward through the d block (participating in a number of avoided crossings along the way).

At the margins of the band structure of Figure 10a, we plot the crystal orbitals corresponding to these σ bands at Γ and Y. At the lowest point at Γ, the orbital consists of bean-shaped lobes on the Co interacting in a σ-bonding fashion along the Co−Co chain. This in-phase combination of Co orbitals is supported by bonding with the sp^2 hybrid orbitals of the surrounding Si/Al atoms. Upon climbing the band to Y, the phase relationships between neighboring cells change so that each Co atom is out-of-phase with its next-nearest Co neighbors. Bonding interactions are retained through the alternation of Co s (with quite a bit of hybridization with the Co d) and Co p contributions along the chain. The two possible phases for this alternation lead to a 2-fold degeneracy at this k-point. Next, after following the band back up to Γ, the orbital takes on the form of a chain of Co p−Co p-bonding interactions.

This progression from s−s bonding, to s−p bonding, and finally to p−p bonding, is familiar from much simpler chain-like structures, for example, the polyethylene polymer. In Figure 10c, we plot the extended Hückel[28] band structure for an idealized version of polyethylene in which, for ease of comparison with the Co1 chain, all the C−C bonds are set to the same length; that is, the bond alternation normally expected has been suppressed. The C−C bonding in this system is largely concentrated in bands 3 and 4 (red), which are σ-bonding, and bands 5 are 6, which span the range from π-bonding to π-antibonding. A comparison of the crystal orbital of the C−C σ-bonding bands with those of the Co−Co σ bands in Figure 10a reveal close similarities in orbital symmetry. While the shapes of individual lobes vary due to the different mixes of Co or C s, p, and d orbitals, the nodal character of the lobes along the axis is identical band by band.

For the C chain of polyethylene, the interpretation of this pair of σ bands is clear: each pair of C atoms is connected via σ bonds, and the bands comprise the full set of symmetrized combinations of these bonds. The analogous character of the σ

dx.doi.org/10.1021/ic302650r | Inorg. Chem. 2013, 52, 3178−3189

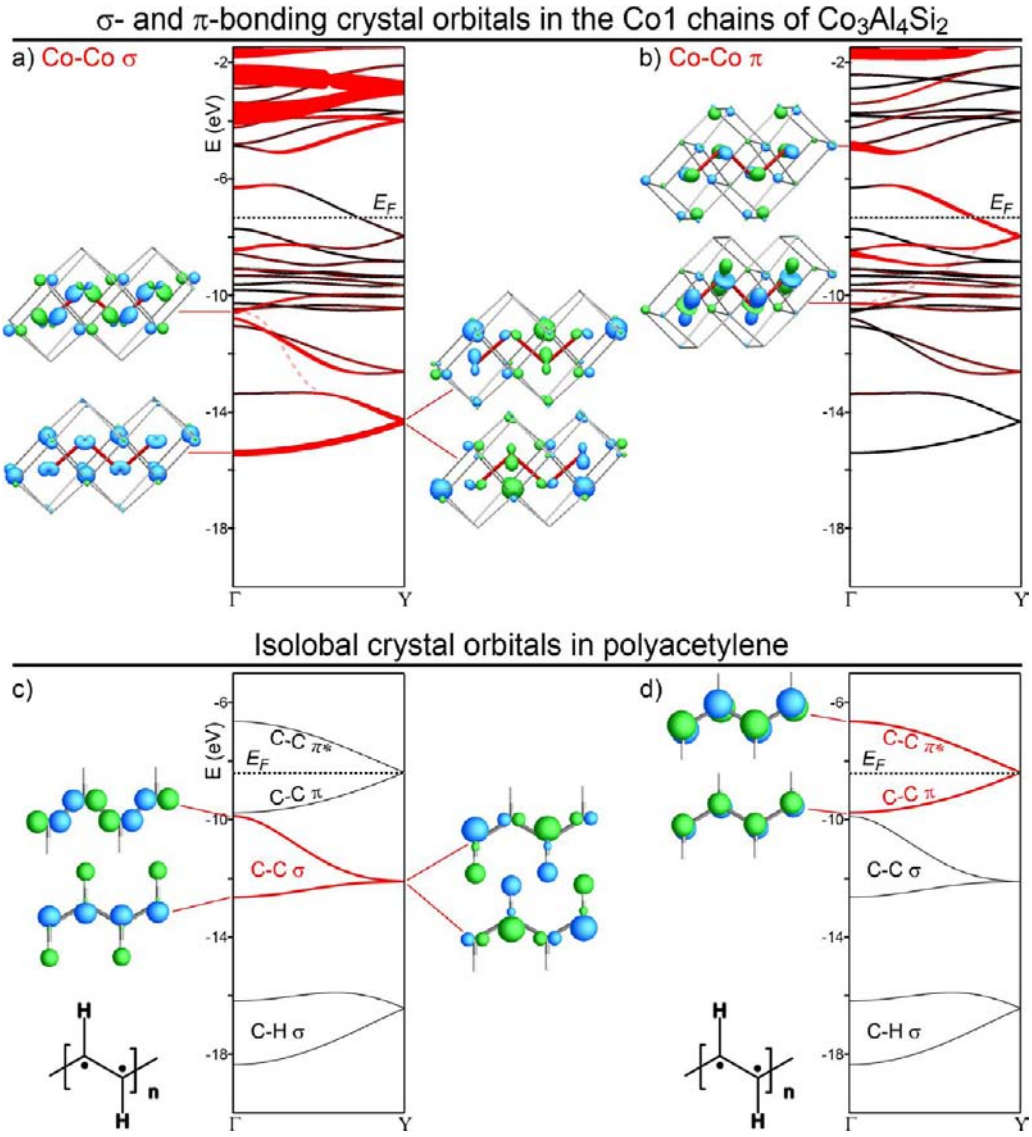

Figure 10. Isolobal relationship between the interactions along the Co backbone of the Co1 chains and the C−C bonding in polyactylene. (a) The band structure of the Co1 chain with its Si/Al neighbors, with the contributions to the crystal orbitals from the σ-sp orbitals represented with red fat-bands (curve thickness proportional to σ contribution). (b) The same Co1 band structure with the contributions from the out-of-plane Co orbitals plotted with red fat-bands. (c, d) The extended Hückel band structure of polyacetylene (without bond alternation), with the C−C σ and C−C π/π^* bands highlighted in red. In all four panels, key crystal orbitals at the special k-points are drawn in the margin.

bands in the Co1 chain brings us to a similar conclusion: the Co atoms of the chain are linked by shared electron pairs through σ interactions. After making this connection, it is important to state an important qualification. As in the Co2 dimers described above, these should not be interpreted as direct through-space interactions. Rather, the in-phase character of the Co atoms allows for favorable multicenter interactions with the bridging Si/Al atoms. The key to electron counting here is to recognize the isolobality of the crystal orbitals to true Co−Co bonds.

From this analysis, we have determined that a shared electron pair occurs at each Co−Co contact. As each Co has two such contacts in the chain, this means that it acquires two electrons from its neighbors. This lowers the number of electrons needed for a filled octadecet to only 16 per Co atom. This is still one electron greater than the 15 electrons/Co at which the pseudogap appears for the Co1 chain. Why is not this extra electron needed?

One hint can be found in the band structure of polyethylene. Each C atom in this chain actually shares three rather than two electron pairs with its C neighbors. The first two pairs occur in the σ bonds we have already discussed. The third, of course, is in the π system. This appears in the band structure as the continuum of states from π-bonding to π-antibonding being half-full (a gap at this electron count would occur if alternation of the bond lengths were permitted—a classic example of a Peierels distortion). The presence of similar π interactions along the Co1 chain could explain the need for only 15 rather than 16 electrons/Co to reach the pseudogap.

In Figure 10c, we explore this possibility with a fat-band analysis of the Co1 chain, in which bands are weighted in red according to the contributions from the out-of-plane Co p orbitals. With the help of these fat-bands, the Co−Co π system can be identified in a pair of bands that straddle the E_F at Γ and bend toward each other across the band structure until they meet at Y. A look at the crystal orbitals at Γ reveals that the

dx.doi.org/10.1021/ic302650r | Inorg. Chem. 2013, 52, 3178−3189

lower and upper branches of this pair correspond, respectively, to the π-bonding and π-antibonding extremes of the Co−Co π system. The E_F of $Co_3Al_4Si_2$ crosses this band structure just after the π-bonding levels are filled, and the π^* levels are beginning to be populated.

The analogy between the Co1 chain and a nonalternating version of polyacetylene thus extends to the π system as well as the Co−Co or C−C σ backbone. With this observation, an explanation for the 15 electron/Co pseudogap in the band structure falls into place: each Co atom shares two electron pairs with its neighbors in a σ fashion, and one electron pair in a π fashion. The sharing of three electron pairs means that each Co needs three fewer electrons to achieve a closed-shell configuration, or 18 − 3 = 15 electrons in total.

$Co_3Al_4Si_2$ as an 18 Electron Compound. From the above analysis, it becomes clear that both the Co1 and the Co2 sites contribute to the pseudogap observed in the DOS of $Co_3Al_4Si_2$. For both sites, filled 18 electron configurations were made possible through the covalent sharing of electrons through multicenter bonding functions that have the same nodal character as true Co−Co σ or π bonds. Each Co2 atom participates in one such covalent bond, allowing for a filled octadecet to be obtained with only 17 electrons/Co2 atom. The Co1 atoms exhibit more extensive Co−Co interactions, sharing three electron pairs with their neighbors. Only 15 electrons are needed for these atoms.

As equal numbers of Co1 and Co2 sites are present in $Co_3Al_4Si_2$, we would predict from this analysis the optimal electron concentration to be (17 + 15)/2 = 16 electrons per Co atom. With our experimentally determined formula of $Co_4Al_{5.58}Si_{2.80}$, the electron concentration is (4 × 9 + 5.58 × 3 + 2.80 × 4)/4 = 15.99 electrons/Co. The composition of the phase is thus in close agreement with this theoretical prediction based on the notion that the Co atoms combine coordination by Si/Al atoms with Co−Co interactions to produce filled octadecets.

The view of $Co_3Al_4Si_2$ as an 18 electron phase offers an explanation for the compound's incommensurate structure. For any set ratio of Si and Al, a set number of Si/Al atoms will be necessary to bring the correct number of electrons to the Co atoms' polyhedra. If the average electron concentration on the Co needs to be 16 for an octadecet, then the Al/Si atoms will be responsible for bringing 7 electrons per Co atom. In the $Co_4Al_{5.58}Si_{2.80}$ composition, the Al/Si ratio is about 2, so that the average electron count per Al/Si atom in the stoichiometry is (2 × 3 + 4)/3 = 3.33. To achieve 7 electrons per Co atom, 7/3.33 = 2.1 Si/Al atoms are required per Co atom, 0.1 Al/Si atoms over the standard 1:2 ratio. In a simple periodic structure, substantial partial occupancies would be required to accommodate the extra 0.1 Si/Al atom. The incommensurate period of the Si3 atoms allows for a smoother way of distributing the correct number of Si/Al atoms among the Co polyhedra.

5. CONCLUSIONS

In this Article, we have presented the incommensurately modulated crystal structure of $Co_3Al_4Si_2$ and illustrated how its bonding can be understood through isolobal analogies to metal−metal bonds in molecular transition metal complexes. The structure contributes to an emerging theme in TM−Si−Al compounds, in which intriguing superstructures are assembled from fragments of the fluorite structure type. $Co_3Al_4Si_2$ builds on this theme, introducing a new layer of complexity: incommensurability. As in the recently determined structure of $Fe_8Al_{17.4}Si_{7.6}$, $Co_3Al_4Si_2$ is based on a rod packing of fluorite-type columns. Layers of interstitial atoms occur between these columns, which are subject to strong modulations. Modeling the structure in 3 + 1D reveals that, in these interstitial layers, one Al/Si site (Si3) adopts a periodicity that is incommensurate with the rest of the structure. The remaining Al/Si site in the layers (Al5) moves in response.

The stability of this arrangement was explored using a DFT-calibrated Hückel model. As in many other TM−main group phases, a DOS pseudogap is apparent at the E_F, indicating that a stable electron count has been achieved. Through cluster models, this was traced to the 18 electron rule. However, key to this connection was the identification of electron pairs being shared between the Co atoms via multicenter bonding orbitals that are isolobal to Co−Co σ or π bonds. With this result, the power of the isolobal analogy to bridge disparate areas of chemistry—from organic molecules to inorganic complexes to transition-metal silicides and intermetallics—is reaffirmed.

From the standpoint of interatomic distances, the importance of shared electron pairs between Co atoms in this compound is startling. The Co−Co distances here, at first glance, seem unremarkable (2.61−2.67 Å), and yet the presence of Si/Al bridges makes these contacts central to the electron counting. This conclusion leads us to wonder how prevalent such delocalized shared electron pairs may be in intermetallics. A fruitful area to pursue this question is the numerous transition metal-main group phases exhibiting unexplained band gaps or DOS pseudogaps.

■ ASSOCIATED CONTENT

Ⓢ Supporting Information

Explanation of skipped reflections; tables of crystallographic data, including atomic coordinates and modulation parameters; figures showing interatomic distances as a function of t; crystallographic information file (CIF) for $Co_3Al_4Si_2$; determination of the 3 + 1D space group of $Co_3Al_4Si_2$ and $\mathbf{b}_{Si3}$; and tables of Hückel parameters used. This material is available free of charge via the Internet at http://pubs.acs.org.

■ AUTHOR INFORMATION

Corresponding Author

*E-mail: danny@chem.wisc.edu.

Notes

The authors declare no competing financial interest.

■ ACKNOWLEDGMENTS

We thank Drs. John Fournelle and Hiromi Konishi (both at the UW−Madison Dept. of Geoscience) for their help with, respectively, the WDS and powder X-ray diffraction measurements. The financial support of the National Science Foundation (NSF) through Grant DMR-1207409 and the Wisconsin Alumni Research Foundation is also gratefully acknowledged. This research involved computer resources supported by NSF Grant CHE-0840494.

■ REFERENCES

(1) (a) Lange, H. *Phys. Status Solidi B* **1997**, *201*, 3. (b) Schmitt, A. L.; Higgins, J. M.; Szczech, J. R.; Jin, S. *J. Mater. Chem.* **2010**, *20*, 223.
(2) (a) Wolf, W.; Bihlmayer, G.; Blügel, S. *Phys. Rev. B* **1997**, *55*, 6918. (b) Lenssen, D.; Bay, H. L.; Mesters, S.; Dieker, C.; Guggi, D.; Carius, R.; Mantl, S. *J. Lumin.* **1998**, *80*, 461. (c) Henrion, W.; Rebien, M.; Birdwell, A. G.; Antonov, V. N.; Jepsen, O. *Thin Solid Films* **2000**,

364, 171. (d) Migas, D. B.; Miglio, L.; Shaposhnikov, V. L.; Borisenko, V. E. *Phys. Status Solidi B* **2002**, *231*, 171.
(3) (a) Nowotny, H. In *The Chemistry of Extended Defects in Non-metallic Solids*; Eyring, L., O'Keeffe, M., Eds.; North-Holland Publishing Co.: Amsterdam, 1970; p 223. (b) Fredrickson, D. C.; Lee, S.; Hoffmann, R.; Lin, J. *Inorg. Chem.* **2004**, *43*, 6151.
(4) (a) Misra, A.; Chu, F.; Mitchell, T. E. *Philos. Mag. A* **1999**, *79*, 1411. (b) Mitchell, T. E.; Misra, A. *Mater. Sci. Eng., A* **1999**, *A261*, 106. (c) Tanaka, K.; Inui, H.; Ohba, T.; Tsutsui, S.; Mizumaki, M. *Mater. Res. Soc. Symp. Proc.* **2004**, *793*, 305. (d) Fredrickson, D. C.; Bostroem, M.; Grin, Y.; Lidin, S. *Chem.—Eur. J.* **2009**, *15*, 8108.
(5) (a) Birkholz, U.; Schelm, J. *Phys. Status Solidi B* **1968**, *27*, 413. (b) Groß, E.; Riffel, M.; Stöhrer, U. *J. Mater. Res.* **1995**, *10*, 34. (c) Takeda, M.; Kuramitsu, M.; Yoshio, M. *Thin Solid Films* **2004**, *461*, 179. (d) Inui, H. *Mater. Res. Soc. Symp. Proc.* **2006**, *886*, 219. (e) Higgins, J. M.; Schmitt, A. L.; Guzei, I. A.; Jin, S. *J. Am. Chem. Soc.* **2008**, *130*, 16086.
(6) Glen, S. In *CRC Handbook of Thermoelectrics*; Rowe, D. M., Eds.; CRC Press: Boca Raton, FL, 1995.
(7) Fredrickson, R. T.; Fredrickson, D. C. *Inorg. Chem.* **2012**, *51*, 10341.
(8) Bertaut, F.; Blum, P. *Compt. Rend.* **1950**, *231*, 626.
(9) Wittmann, A.; Burger, K. O.; Nowotny, H. *Monatsh. Chem.* **1962**, *93*, 674.
(10) (a) Tobola, J.; Pierre, J.; Kaprzyk, S.; Skolozdra, R. V.; Kouacou, M. A. *J. Magn. Magn. Mater.* **1996**, *159*, 192. (b) Tobola, J.; Pierre, J.; Kaprzyk, S.; Skolozdra, R. V.; Kouacou, M. A. *J. Phys.: Condens. Matter* **1998**, *10*, 1013. (c) Jung, D.; Koo, H. J.; Whangbo, M. H. *J. Mol. Struct.: THEOCHEM* **2000**, *527*, 113. (d) Tobola, J.; Pierre, J. *J. Alloys Compd.* **2000**, *296*, 243. (e) Kandpal, H. C.; Felser, C.; Seshadri, R. *J. Phys. D: Appl. Phys.* **2006**, *39*, 776.
(11) Schmid Fetzer, R. In *Ternary Alloys: A Comprehensive Compendium of Evaluated Constitutional Data and Phase Diagrams*; Petzow, G., Effenberg, G., Eds.; VCH: Weinheim, Germany, 1991; Vol. *4*, p 254.
(12) (a) Burger, K. O.; Wittmann, A.; Nowotny, H. *Monatsh. Chem.* **1962**, *93*, 9. (b) Richter, K. W.; Prots, Y.; Grin, Y. *Inorg. Chem.* **2005**, *44*, 4576. (c) Richter, K. W.; Prots, Y. *Z. Kristallogr. - New Cryst. Struct.* **2006**, *221*, 115. (d) Richter, K. W.; Prots, Y. *Z. Kristallogr. - New Cryst. Struct.* **2006**, *221*, 112. (e) Wu, X.; Latturner, S.; Kanatzidis, M. G. *Inorg. Chem.* **2006**, *45*, 5358.
(13) German, N. V.; Zavodnik, V. E.; Yanson, T. I.; Zarechnyuk, O. S. *Kristallografiya* **1989**, *34*, 738.
(14) Hoffmann, R. *Angew. Chem., Int. Ed.* **1982**, *21*, 711.
(15) Petříček, V.; Dušek, M.; Palatinus, L. *Jana2006: The Crystallographic Computing System*; Institute of Physics: Praha, Czech Republic, 2006.
(16) (a) Oszlányi, G.; Sütő, A. *Acta Crystallogr.* **2004**, *A60*, 134. (b) Palatinus, L. *Acta Crystallogr.* **2004**, *A60*, 604. (c) Oszlányi, G.; Sütő, A. *Acta Crystallogr.* **2005**, *A61*, 147.
(17) Palatinus, L.; Chapuis, G. *J. Appl. Crystallogr.* **2007**, *40*, 786.
(18) Momma, K.; Izumi, F. *J. Appl. Crystallogr.* **2011**, *44*, 1272.
(19) (a) Kresse, G.; Furthmüller, J. *Phys. Rev. B* **1996**, *54*, 11169. (b) Kresse, G.; Furthmüller, J. *Comput. Mater. Sci.* **1996**, *6*, 15.
(20) Perdew, J. P.; Chevary, J. A.; Vosko, S. H.; Jackson, K. A.; Pederson, M. R.; Singh, D. J.; Fiolhais, C. *Phys. Rev. B* **1992**, *46*, 6671.
(21) (a) Blöchl, P. E. *Phys. Rev. B* **1994**, *50*, 17953. (b) Kresse, G.; Joubert, D. *Phys. Rev. B* **1999**, *59*, 1758.
(22) Stacey, T. E.; Fredrickson, D. C. *Dalton Trans.* **2012**, *41*, 7801.
(23) Landrum, G. A. *YAeHMOP: Yet Another Extended Hückel Molecular Orbital Program*, Version. 3.0. YAeHMOP is freely available on the WWW at: http://sourceforge.net/projects/yaehmop/.
(24) (a) Janssen, T.; Janner, J.; Looijenga-Vos, A.; de Wolff, P. M. In *International Tables for Crystallography*; Prince, E., Ed.; Kluwer Academic Publishers: Dordrecht, 2004; Vol. *C*, p 907. (b) van Smaalen, S. *Z. Kristallogr.* **2004**, *219*, 681.
(25) Yamamoto, A. *Acta Crystallogr.* **1993**, *A49*, 831.
(26) Taylor, A.; Floyd, R. W. *Acta Crystallogr.* **1950**, *3*, 285.
(27) Hoffmann, R. *Solids and Surfaces: A Chemist's View of Bonding in Extended Structures*; VCH Publishers: New York, 1988.
(28) Hoffmann, R. *J. Chem. Phys.* **1963**, *39*, 1397.